Microscopic descriptions of exotic nuclei and their reactions

S. Karataglidis
CEA, Département de Physique Théorique Appliquée, Boîte Postale 12, F-91680
Bruyères-le-Châtel, France

Abstract

With the availability of data which allow one to probe the microscopic properties of exotic nuclei, more attention is turning to many-body descriptions of nuclei towards the drip lines. In such cases, special care is needed in the treatment of the loosely bound nucleons in order to obtain densities which reflect the extensivity of those systems. The problem is addressed in reference to data for the scattering of ^{6,8}He and ^{9,11}Li from hydrogen as well as charged photopion reactions. Methods for handling the density are discussed.

I. INTRODUCTION

The microscopic descriptions of exotic nuclei, and the problems involved as one approaches the drip lines, is a topic of current interest. The light mass proton/neutron rich nuclei are particularly suited for study as a number of these may be formed as radioative beams with which to perform experiments. Their scattering from hydrogen targets is especially interesting as that translates to proton scattering in the inverse kinematics. With the recent advances in folding models [1], the matter densities of exotic nuclei may be studied by elastic and inelastic scattering from hydrogen in a manner consistent with that of electron scattering. Other complementary data are available, notably charge exchange reactions (see, for example, [2, 3]), as are β-decay measurements (for example [4, 5]).

To analyse such complementary reactions, one must begin with a credible model of structure and one, preferably, which is nucleon-based. That allows for the same underlying density matrix elements to be used in the analyses of data. Calculations from those models, when tested against spectra and ground state properties, yield the one-body density matrix elements (OBDME) from which one is able to construct the pertinent scattering and/or reaction matrix elements.

Herein, we consider scattering from hydrogen for a number of neutron-rich nuclei: the light exotics ^{6,8}He and ^{9,11}Li, as well as exotic isotopes of Ca. The model used is the g-folding model of the Melbourne Group [1]. That model utilises effective nucleon-nucleon (NN) interactions obtained from g matrices in infinite matter; solutions of the Bruckner-Bethe-Goldstone equations. The densities, with which these effective interactions are used to specify the microscopic optical potentials, are obtained by folding the OBDME with an appropriate set of single particle (SP) wave functions. Those OBDME are also used in analyses of complementary data as a test of the structure.

For the SP functions, one usually assumes harmonic oscillator (HO) or Woods-Saxon (WS) wave functions in the analyses of data. The latter allow for the specification of the densities of loosely bound systems (whether halo or skin) by setting the binding energies of the valence orbits to the appropriate single-nucleon separation energies. Another scheme allows for modification of oscillator wave functions in a minimal fashion to obtain similar extensions. Those SP functions based on the Local Scale Transformations (LST) of the radial coordinate in HO functions are also discussed.

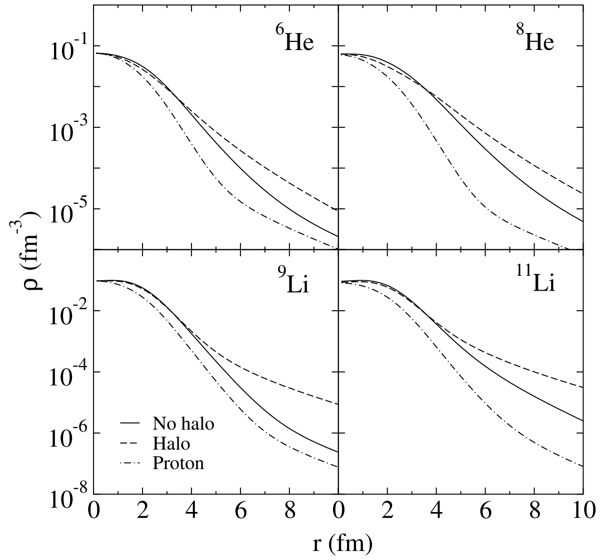

FIG. 1: Densities for ^{6}He, ^{8}He, ^{9}Li, and ^{11}Li, as obtained from the models discussed in the text.

II. NUCLEAR STRUCTURE

Complete $(0+2+4)\hbar\omega$ shell models with the Arizona G matrix shell model interaction [6] have been used to obtain the OBDME for ^{6,8}He, while a complete $(0+2)\hbar\omega$ model with the WBT interaction of Warburton and Brown [7] was used to obtain the OBDME for ^{9,11}Li. To specify the density in the case of the halo nuclei, the binding energies of the WS SP wave functions for the valence neutron orbits were set to the single neutron separation energies: 1.8 MeV for ^{6}He and 0.5 for ^{11}Li. A standard set of WS functions were used for ^{8}He and ^{9}Li to specify the nonhalo (skin) aspects of those nuclei while an artifical "halo" was induced in those cases by setting the valence neutron orbits also to a binding energy of 0.5 MeV. The densities so obtained are in Fig. 1. In each case, the extensions in the neutron densities as given by the WS SP wave functions are clearly seen; those arise with a corresponding depletion of strength in the core region.

The Ca isotopes form a comparative study. Alternative models predicated on Hartree-Fock (HF) and the RPA have been incorporated into the g-folding model, allowing for the use of densities from realistic models of heavy nuclei to be used in analyses. The use of Skyrme-Hartree-Fock has been demonstrated in the case of ^{40}Ca and ^{208}Pb [8, 9], wherein the skin thickness of ^{208}Pb was determined to be 0.17 fm from analyses of elastic nucleon-nucleus scattering. This is in line with determinations from other model analyses (see, for example, [10]).

III. COORDINATE SPACE OPTICAL POTENTIAL

A realistic model of the nucleon-nucleus (NA) optical potential should be predicated upon an appropriate effective NN interaction and such are the g matrices of the NN interaction; solutions of the Bruckner-Bethe-Goldstone equations. For the calculations presented herein, we have used the Bonn B NN interaction [11]. The infinite matter g matrices are obtained in momentum space and are mapped to the finite nucleus using a local density approximation.

Those effective interactions are transformed to a coordinate space representation for use in the DWBA98 program of Raynal [12] to calculate scattering observables.

To obtain the NA optical potential the effective NN interaction is folded with the OBDME obtained from the relevant model of structure together with the appropriate SP wave functions. The OBDME are of the form (with α specifying the set $\{n, l, j\}$ and $\tilde{a}_{\alpha m} = (-1)^{j-m} a_{\alpha -m}$)

$$S_{\alpha\alpha' I} = \left\langle J_f \left\| \left[a^{\dagger}_{\alpha'} \times \tilde{a}_{\alpha} \right]^I \right\| J_i \right\rangle \to \left\langle J \left\| \left[a^{\dagger}_{\alpha'} \times \tilde{a}_{\alpha} \right]^I \right\| J \right\rangle \tag{1}$$

in the case of elastic scattering from a target of spin J. A distorted wave approximation may be used to calculate the scattering matrix elements for which $I \neq 0$. The optical potential obtained by the folding process for elastic scattering takes the form

$$\begin{aligned} U(\boldsymbol{r}, \boldsymbol{r}'; E) &= \delta(\boldsymbol{r} - \boldsymbol{r}') \sum_i n_i \int \varphi_i^*(\boldsymbol{s}) g_D(\boldsymbol{r}, \boldsymbol{s}; E) \varphi_i(\boldsymbol{s}) \, d\boldsymbol{s} \\ &\quad + \sum_i n_i \; \varphi_i^*(\boldsymbol{r}) \; g_E(\boldsymbol{r}, \boldsymbol{r}'; E) \; \varphi_i(\boldsymbol{r}') \\ &= U_D(\boldsymbol{r}; E) \; \delta(\boldsymbol{r} - \boldsymbol{r}') + U_E(\boldsymbol{r}, \boldsymbol{r}'; E) \; , \end{aligned}$$

where n_i are the occupation numbers (obtained from the relevant OBDME), and φ are the SP functions. Those may be taken to be of HO or WS form, or obtained from the HF models directly in those cases where the structure is specified by HF or RPA within the HF basis. An alternative is to transform the oscillator functions themselves to reflect the correct long-range behaviour, as described in the next section.

IV. LOCAL SCALE TRANSFORMATIONS

A scheme exists whereby harmonic oscillator functions may be transformed to decay exponentially at large distance consistent with the binding energy of the state [13–16]. This local scale transformation (LST) of the radial variable in oscillator functions represents a minimal transformation of the structure whereby the internal part of the model nuclear density remains largely intact, while the extension of the density is consistent with binding.

An LST of the form $r = f(s)$ replaces an original wave function $u(r)$ by a new one $v(r)$ defined by the isometric transform

$$v(r) = \sqrt{\frac{df}{dr}} u\left[f(r)\right] \tag{2}$$

where $f(r)$ must be real and monotonically increasing when r runs from 0 to ∞. Also, it satisfies two boundary conditions, namely $f(0) = 0$ and $f(r) \to \infty$ as $r \to \infty$. The transformation preserves the norm,

$$\int_0^{\infty} ds \; v(s) v^*(s) = \int_0^{\infty} ds \; \frac{df}{ds} u\left[f(s)\right] u^*\left[f(s)\right] = \int_0^{\infty} dr \; u(r) u^*(r) \tag{3}$$

under the change of variable $r = f(s)$. For radial wave functions, one must slightly modify the transform according to

$$v(r) = \frac{f(r)}{r} \sqrt{\frac{df}{dr}} u\left[f(r)\right] = s(r) u\left[f(r)\right] \; , \tag{4}$$

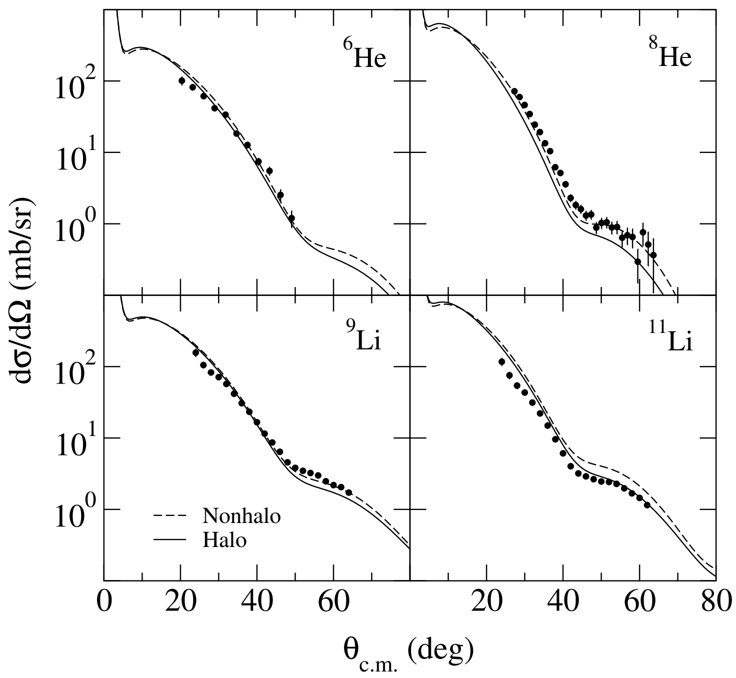

FIG. 2: Elastic scattering for the scattering of 71A MeV ^{6}He and ^{8}He, and 62A MeV ^{9}Li and ^{11}Li from hydrogen.

where $s(r)$ is the wave function scale. With b and μ denoting the oscillator parameter and (bare) nucleon mass respectively the choice of f induces a change in structure

$$\exp\left(-\frac{r^2}{2b^2}\right) \Rightarrow \exp\left[-r\sqrt{\frac{2\mu\varepsilon}{\hbar^2}}\right]. \tag{5}$$

Hence, the boundary condition as $r \to \infty$ requires

$$f(r) \to \gamma\sqrt{r}, \text{ with } \gamma = b\left[\frac{8\mu\varepsilon}{\hbar^2}\right]^{\frac{1}{4}}, \tag{6}$$

while $f(r) \to r$ as $r \to 0$ seems the most appropriate choice satisfying the other boundary.

To ensure the normalisation remains real, we choose the following transform (harmonic mean form),

$$f(r) = \left[\frac{1}{r^{-m} + \left(\gamma\sqrt{r}\right)^{-m}}\right]^{\frac{1}{m}} \tag{7}$$

where m is the mean of the transform. Typical values range from $m = 2$ to 20; we choose $m = 8$ as an example.

V. RESULTS

Results for elastic scattering of ^{6,8}He and ^{9,11}Li from hydrogen are presented in Fig. 2. The analyses indicate a halo in ^{11}Li, and no halos in ^{8}He and ^{9}Li, but are not conclusive in the case of ^{6}He. Subsequent analyses of elastic and inelastic (to the 2^+ state) 40A MeV

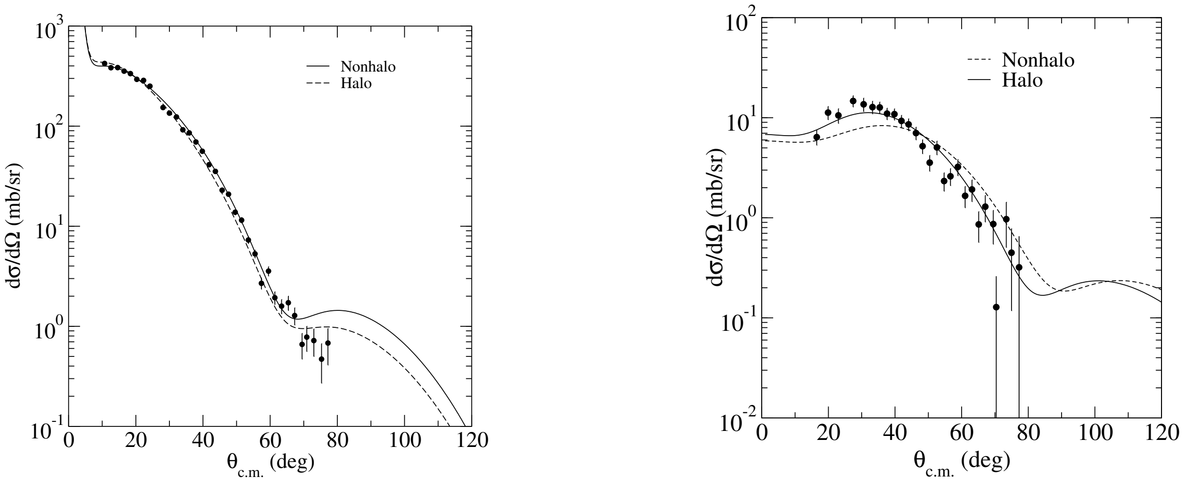

FIG. 3: Elastic (left) and inelastic (right) to the 2^+ (1.8 MeV) state scattering of $40A$ MeV ^{6}He from hydrogen.

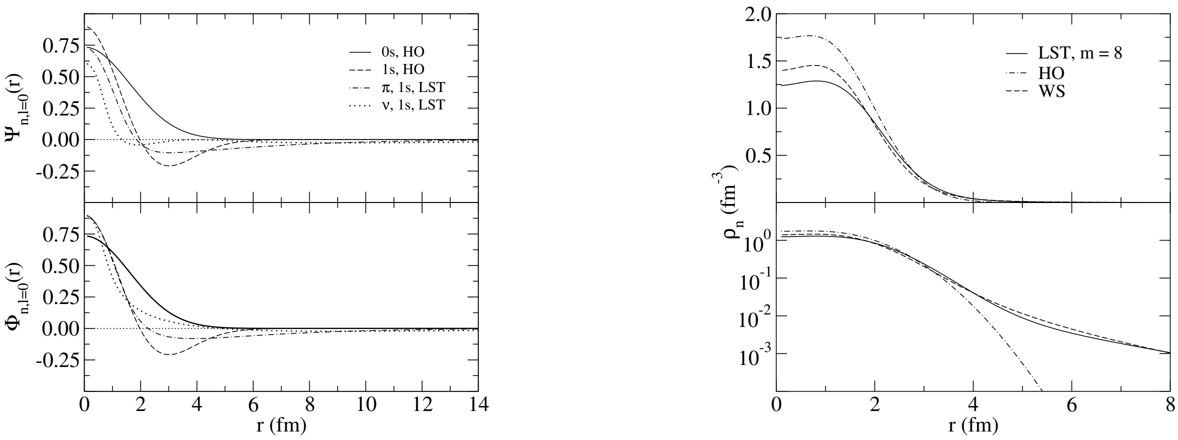

FIG. 4: $0s$ and $1s$ wave functions (left) and neutron densities (right) for ^{11}Li.

^{6}He scattering from hydrogen [17], presented in Fig. 3, indicate explicitly the halo in ^{6}He. However, analyses of existing data from the complementary $^6\mathrm{Li}(\gamma,\pi^+)^6\mathrm{He}_{gs}$ reaction [3] and β-delayed deuteron emission from ^{6}He [4] still give some doubt. A remeasurement of the $^6\mathrm{Li}(\gamma,\pi^+)^6\mathrm{He}_{gs}$ reaction has been proposed at both Mainz and MAXLab. A remeasurement of the *beta*-decay is also desirable.

To illustrate the effect on the density of the use of LST functions, Fig. 4 displays the $0s$ (binding energy of 33 MeV) and $1s$ proton (binding energy 2.9 MeV) and neutron (binding energy 0.5 MeV) wave functions for ^{11}Li, in both the oscillator and LST forms, along with the neutron densities as obtained using HO, WS, and LST SP wave functions. The LST $0s$ and $1s$ functions in the upper part of the figure are those after the re-orthogonalisation necessary to ensure that the correct binding energies apply for both orbits. Both the WS and LST densities are extensive compared to that obtained using HO functions, reflecting the halo nature of that nucleus. And, as observed in Fig. 1, the density in the core region is depleted in the case of the WS and LST models to ensure conservation of particle number.

Fig. 5 displays the elastic scattering cross section for ^{11}Li at 62 MeV, as obtained using

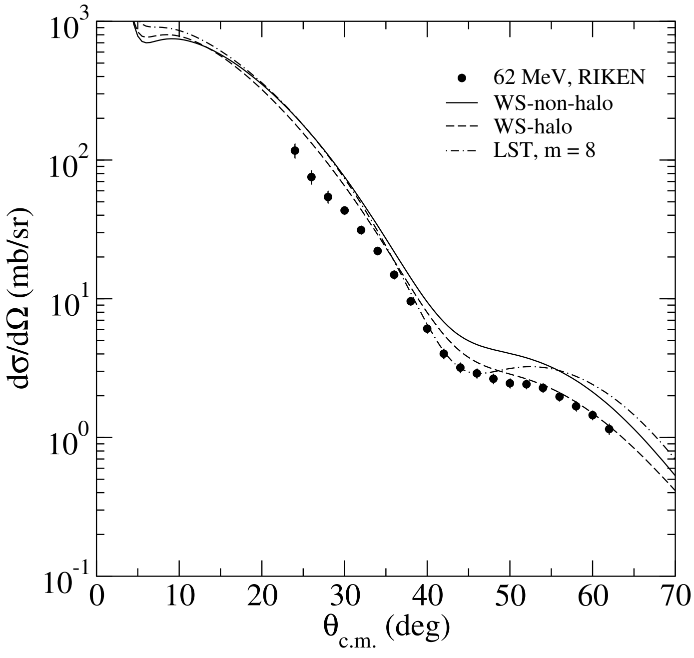

FIG. 5: Differential cross section for the elastic scattering of ^{11}Li from hydrogen at $62A$ MeV.

the WS halo and non-halo models ([3] and references cited therein), together with the LST result, in comparison to the data [18]. The WS-halo and LST models were obtained using the same set of binding energies. There is some agreement between the two results, and the LST result is a correction to that of the non-halo model. However, the agreement between the LST model and data fails in the large angle region.

The differential cross sections for the elastic scattering of 65 MeV protons and neutrons from ^{40}Ca is displayed in Fig. 6. Therein, the data [19, 20] are compared to the results of calculations made using the Skyrme-Hartree-Fock model of Brown [8] and also the RPA model using the Gogny D1S force [21]. Both models show excellent agreement with the data and with each other. Also displayed is the LST result for proton scattering. That result also shows excellent agreement with data indicating that the LST is well-behaved for this test case. The discrepancy with the neutron scattering data at $\sim 30°$ has been noted previously [22]; a remeasurement of this cross section is desirable.

Brown [23] has presented results showing that not only is ^{52}Ca doubly magic but so also is ^{54}Ca. These are based on shell model calculations made using the GXPF interaction [24]. One may ask whether this observation is reflected in the neutron density and so a preliminary calculation of the proton elastic scattering cross sections at 65 MeV has been made for scattering from several Ca isotopes (^{40}Ca through to ^{54}Ca) using those shell model wave functions [25]. The results are displayed in Fig. 7. The cross section moves to more forward angles with increasing mass, as expected. However, the trend is not quite linear as the increase from ^{52}Ca to ^{54}Ca does not produce as much of a shift as is apparent for the lighter isotopes.

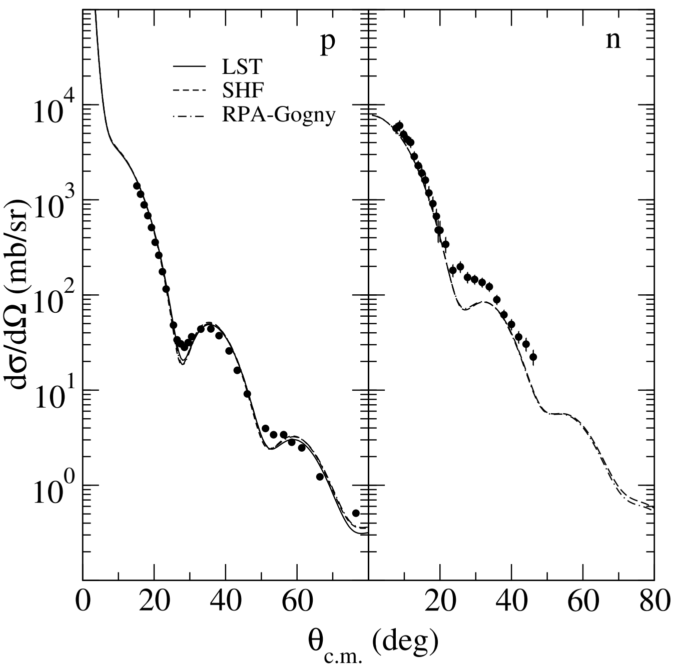

FIG. 6: Differential cross sections for the elastic scattering of 65 MeV protons and neutrons from ^{40}Ca.

VI. CONCLUSIONS

The Melbourne g-folding model of nucleon-nucleus scattering has now been extended to allow for analyses of scattering from heavy nuclei using realistic wave functions. Results have been presented for the elastic scattering of nucleons from ^{40}Ca using Skyrme-Hartree-Fock and RPA wave functions. Those results show excellent agreement with available data; they show promise for the use of such wave functions elsewhere (see [9] herein).

The model has successfully been used also in analyses of complementary reaction data involving exotic nuclei in order to elicit details of the underlying microscopic nuclear structure. While existing scattering data have confirmed the existence of a halo in ^{6}He, complementary $^6\text{Li}(\gamma, \pi^+)^6\text{He}_{gs}$ and β-decay data would seem to indicate otherwise. New measurements of the $^6\text{Li}(\gamma, \pi^+)^6\text{He}_{gs}$ cross section are planned; a third measurement of the *beta*-delayed deutron emission from ^{6}He is desirable.

For the analyses of data involving halo nuclei from a microscopic standpoint, one requires the use of more realistic SP wave functions which reflect the extensive densities of those systems, preferably in conjunction with complete large space shell models. Heretofore this has been achieved using a set WS functions with binding energies of the relevant orbits for the valence nucleons set to the single nucleon separation energy. To achieve a closer connection to the underlying (oscillator-based) nuclear structure, the LST functions may be used and results from those analyses show promise. However, in order to achieve better agreement with data, a better understanding of the binding energies is required.

One hopes that (complementary) experiments eliciting microscopic details of the structure of exotic nuclei will continue to be made. This will allow further investigation of how novel

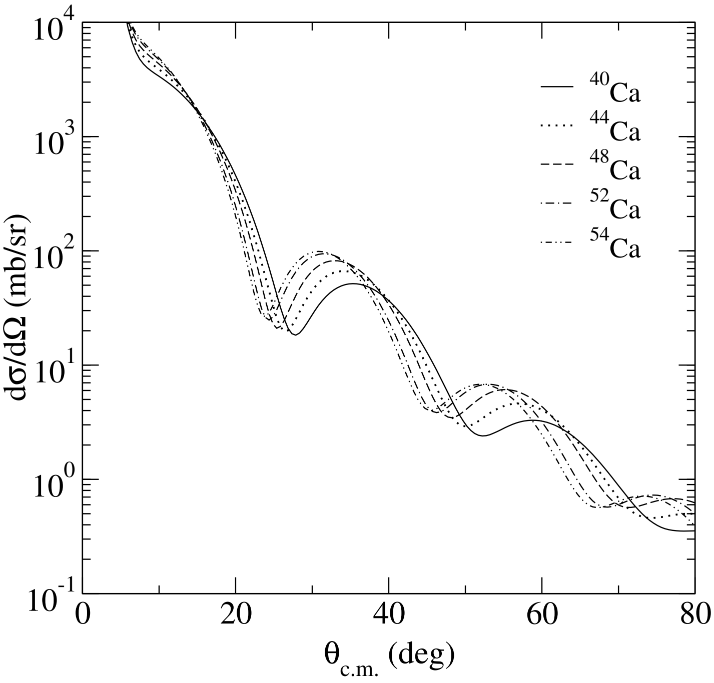

FIG. 7: Differential cross sections for the elastic scattering of 65 MeV protons from the listed isotopes of Ca.

structures such as the halo become manifest in many-body systems.

---

[1] K. Amos, P. J. Dortmans, H. V. von Geramb, S. Karataglidis, and J. Raynal, Adv. in Nucl. Phys. **25**, 275 (2000), and referencees cited therein.
[2] S. Karataglidis and C. Bennhold, Phys. Rev. Lett. **80**, 1614 (1998).
[3] S. Karataglidis, P. J. Dortmans, K. Amos, and C. Bennhold, Phys. Rev. C **61**, 024319 (2000).
[4] D. Anthony et al., Phys. Rev. C **65**, 034310 (2002).
[5] M. S. Curtin et al., Phys. Rev. Lett. **56**, 34 (1986).
[6] D. C. Zheng, B. R. Barrett, J. P. Vary, W. C. Haxton, and C.-L. Song, Phys. Rev. C **52**, 2498 (1995).
[7] E. K. Warburton and B. A. Brown, Phys. Rev. C **46**, 923 (1992).
[8] S. Karataglidis, K. Amos, B. A. Brown, and P. K. Deb, Phys. Rev. C **65**, 044306 (2002).
[9] K. Amos, contribution to this conference.
[10] B. C. Clark, L. J. Kerr, and S. Hama, Phys. Rev. C **67**, 054605 (2003).
[11] R. Machleidt, K. Holinde, and C. Elster, Phys. Rep. **149**, 1 (1987).
[12] J. Raynal, *computer program dwba98, nea 1209/05* (1998).
[13] I. Z. Petkov and M. V. Stoitsov, Sov. J. Nucl. Phys. **37**, 692 (1983).
[14] M. V. Stoitsov, W. Nazarewicz, and S. Pittel, Phys. Rev. C **58**, 2092 (1998).
[15] S. Pittel and M. V. Stoitsov, Phys. Atomic Nuclei **64**, 1055 (2001).
[16] K. Amos, B. G. Giraud, and S. Karataglidis, submitted to Phys. Rev. C, 2003.
[17] A. Lagoyannis et al., Phys. Lett. **B518**, 27 (2001).
[18] C.-B. Moon et al., Phys. Lett. **297B**, 39 (1992).

[19] H. Sakaguchi et al., Phys. Rev. C **26**, 944 (1982).
[20] E. L. Hjort et al., Phys. Rev. C **50**, 275 (1994).
[21] J. Dechargeé and D. Gogny, Phys. Rev. C **21**, 1568 (1980).
[22] S. Karataglidis and M. B. Chadwick, Phys. Rev. C **64**, 064601 (2001).
[23] B. A. Brown, contribution to this conference.
[24] M. Honma, T. Otsuka, B. A. Brown, and T. Mizusaki, Phys. Rev. C **65**, 061301(R) (2002).
[25] B. A. Brown, private communication.